Electronic Supplementary Material (ESI) for Chemical Communications.

Supporting Information

Insight into the effect of additives widely used in lithium-sulfur batteries

Salatan Duangdangchote[a,b], Atiweena Krittayavathananon[a,b], Nutthaphon Phattharasupakun[a,b], Nattanon Joraleechanchai[a,b] and Montree Sawangphruk[a,b,*]

Centre of Excellence for Energy Storage Technology (CEST), Department of Chemical and Biomolecular Engineering, School of Energy Science and Engineering, Vidyasirimedhi Institute of Science and Technology, Rayong 21210, Thailand

Corresponding author. E-mail address: montree.s@vistec.ac.th (M. Sawangphruk).

Supplementary Note 1.

The reactive molecular dynamics (RMD) simulations were developed by the atomistic force-field methods through the reactive force-field (ReaxFF)[1-3] simulations for the relations between C, H, O, N, S, F, Cl and Li atoms, and the interactions were trained for lithium-sulphur battery materials[4-6]. The relations between Li and Cl are also described in Supplementary Note 3. Each cell was built into the lithium anode, and the electrolyte components. The lithium anode was constructed from the Li body-centred cubic (bcc) structure with a lattice parameter of 3.490 Å[7], and then, the bulk structure was cut along the (100) directions to build a surface slab with cell parameters of 55.8 Å × 27.9 Å × 69.8 Å. The periodic boundary condition (PBC) was applied along the *X* and *Y* directions, where the bottom 4 layers of Li(100) were fixed at bulk position, the elastic wall was also built at Z = 0 Å to avoid the interaction between the bottom surface of Li(100) and electrolyte components due to PBC in *Z*-direction. The electrolyte components were packed using PackMol. After assembling all of regions, the simulation cell parameters were changed to 55.8 Å × 27.9 Å × 169.8 Å. The initial configurations are also shown in Fig. S1. The reactions between anode and electrolyte components take place on the top of Li(100) surface. The simulations were carried out with a canonical ensemble at the constant number of particles N, volume V, and temperature T (NVT) with the Nosé-Hoover chain (NHC)[8] thermostat with a damping parameter of 0.01 fs^{-1}. The time step of 0.25 fs and the temperature of 298 K were applied for entire RMD simulations.

The density functional theory (DFT) investigations in this article were performed by the Gaussian16 computational package[9]. Full optimizations, geometries and property calculations for the total energies were accounted by unrestricted the hybrid meta generalized gradient approximation (meta-GGA)[10] with Minnesota class exchange-correlation functional M06-2X[11] and the polarized double ζ basis set 6-31G(d,p) was set for all atoms. The convergence thresholds for self-consistency-field (SCF) was set at 10^{-6} Hartree. The counterpoise method[12] (CP) was used to estimate the corrections of the basis set superposition error (BSSE) to obtain more reliable interaction energies. All stationary points were characterized as no imaginary frequencies by calculation using the same level of theory. The calculated relative binding (E_b) energies were defined as follows:

$$E_b = E_{C/LPSs} - E_C - E_{LPSs}$$

where $E_{C/LPSs}$, E_C, and E_{LPSs} are the total energies of the adsorbed LPSs molecule on the cluster, the clean cluster, and the isolated LPSs molecule, respectively. The natural bond orbital (NBO)[13] method was also used to analyse the charge transfer between LPSs and relevant cluster species. The charge transfer from the lithium bond interaction was estimated as follows[14]:

$$\Delta\rho = \left|\rho_{CFP/LPSs} - \rho_{LPSs}\right|$$

where $\rho_{C/LPSs}$and ρ_{LPSs} are the net charge of the adsorbed LPSs on the cluster and isolated LPSs, respectively.

Supplementary Note 2.

In this work, we performed additional reactive force field against the DFT calculations for describing bond dissociation for the Li-Cl. The DFT parameterized for training data were carried out in the Amsterdam Density Functional (ADF) suite with the B3LYP hybrid functional along with the TZDP basis set. To parameterize ReaxFF bond energy data, we carried out DFT calculations on Li-Cl bond dissociation in a LiCl molecule. In order to obtain dissociation profiles, bond restraint was applied in the atom pair of interest during geometry relaxation. Bond distances were varied from 1.35 to 9 Å. Fig. S0 shows the comparison of the ReaxFF and DFT results. The ReaxFF agreeably reproduces full dissociation profile, especially, near the equilibrium region. This parameter is in good agreement with the DFT values.

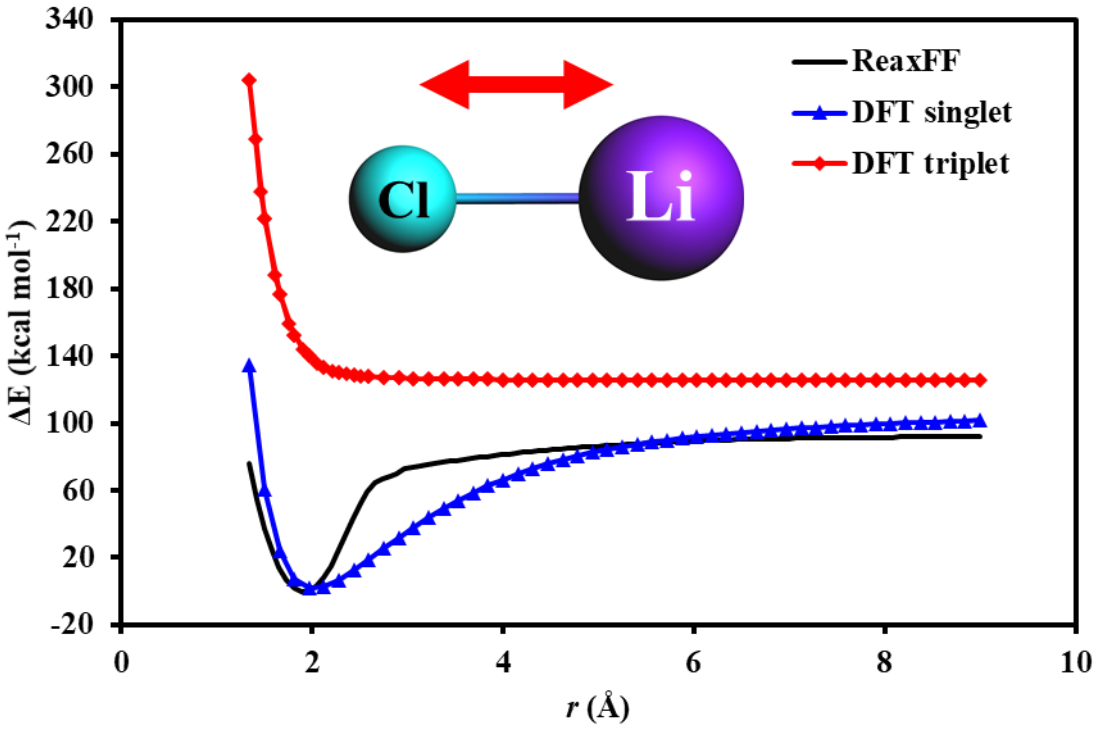

Fig. S0. Comparison of the ReaxFF and DFT data for a Li-Cl bond dissociation in LiCl.

Supplementary Note 3.

The electrochemical performances of LSBs with different additives were tested using 2032-type coin cells with lithium metal chips as a counter electrode, poly(ethylene) (PE; Celgard 3501) membrane was used as a separator. The cathode materials were prepared from a conventional slurry-coating process by mixing Sulphur (S_8; Alfa Aesar, 99.5%), Carbon black (Super P conductive; Alfa Aesar, 99+%), and poly(vinylidene fluoride) (PVDF; Aldrich) binder in a mass ratio of 6:3:1, and homogenized in N-methyl-2-pyrrolidone (NMP; QREC) to form slurries. The slurries were uniformly coated on pristine aluminium (Al) foil substrates and dried at 60 °C for 8 hours. The mass loading on each electrode was controlled to be 2-3 mg cm^{-2}. The electrolyte additives were used 0.1 M of lithium nitrate ($LiNO_3$; Aldrich, ReagentPlus®), lithium bromide (LiBr; TCI, >99%), lithium iodide (LiI; Aldrich, 99.99%), lithium tetrafluoroborate ($LiBF_4$; TCI, 98.0%), and lithium perchlorate ($LiClO_4$; Aldrich, 99.99%). Each additive was mixed with 1M bis(trifluoromethane)sulfonimide lithium salt (LiTFSI; Aldrich, 99.95%) in 1:1 v/v of 1,3-dioxolane (DOL; Aldrich) and 1,2-dimethoxyethane (DME; Aldrich) mixture solvents. The galvanostatic charge/discharge measurements were performed on NEWARE BTS-CT3008 (Neware Technology, Shenzhen, China) at a constant current density of 0.1C.

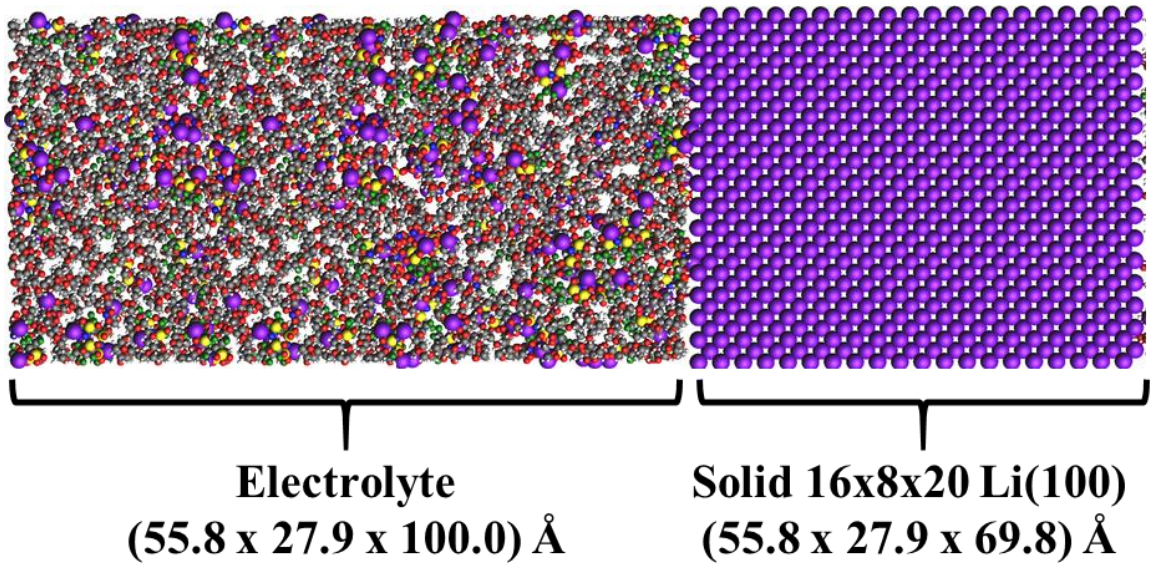

Fig. S1. Initial configuration of the simulation cell with $LiNO_3$. Color for Li: purple, C: gray, H: white, N: blue, F: green, and S: yellow.

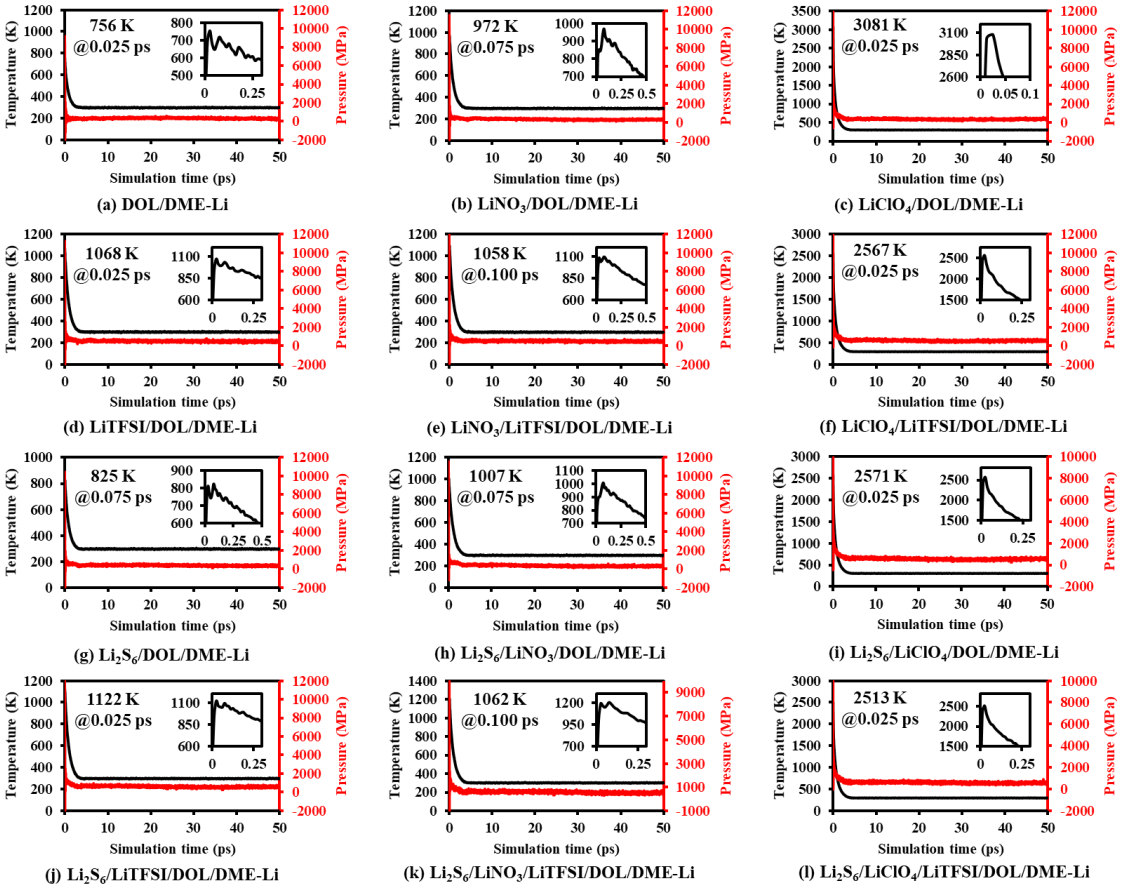

Fig. S2. System temperature profile with simulation time for various simulation system.

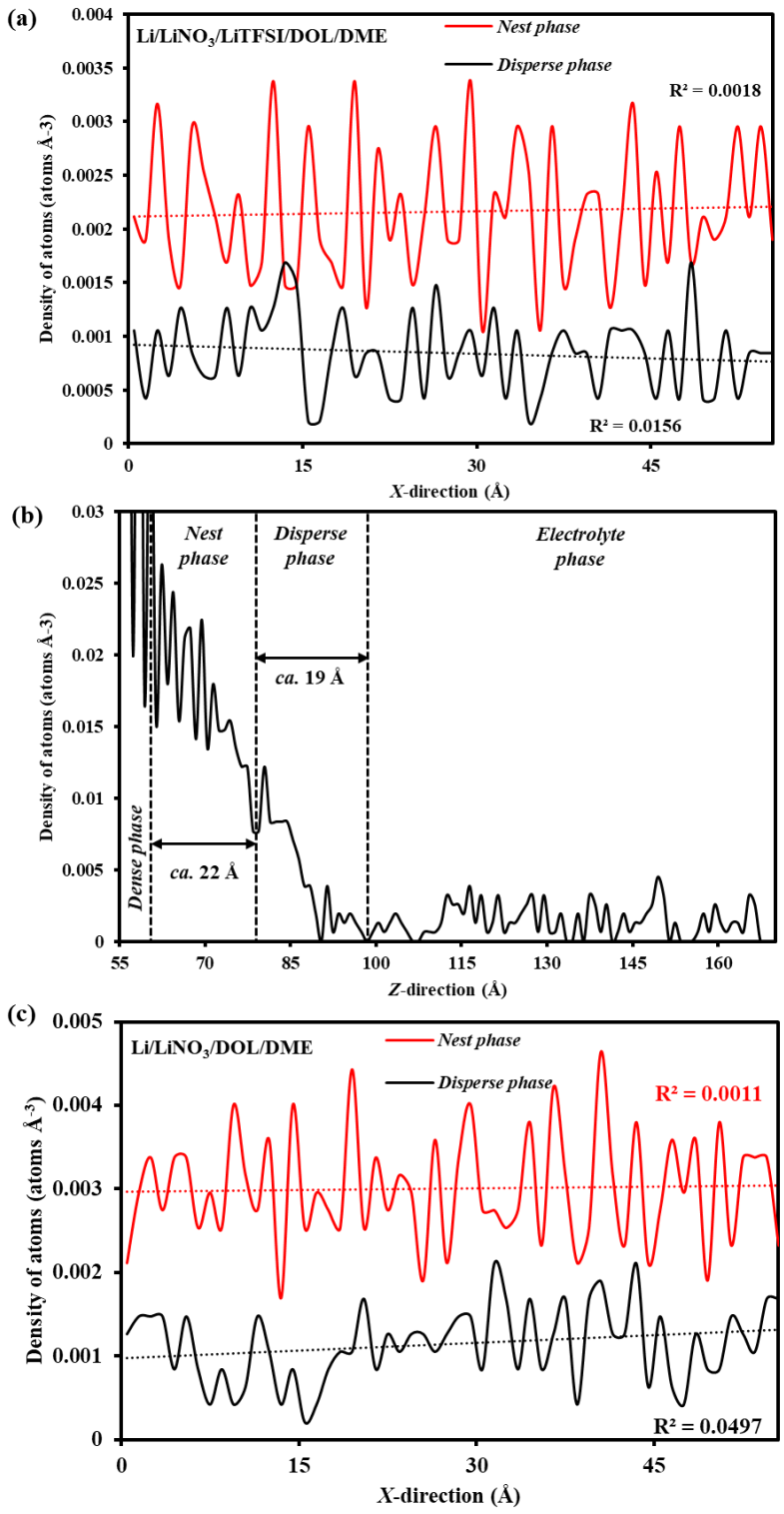

Fig. S3. Density profiles of Li atoms in (a) *X*-, (b) *Z*-directions for simulation system $LiNO_3$/LiTFSI/DOL/DME, and (c) *X*-directions for simulation system $LiNO_3$/DOL/DME at 50 ps of simulation time.

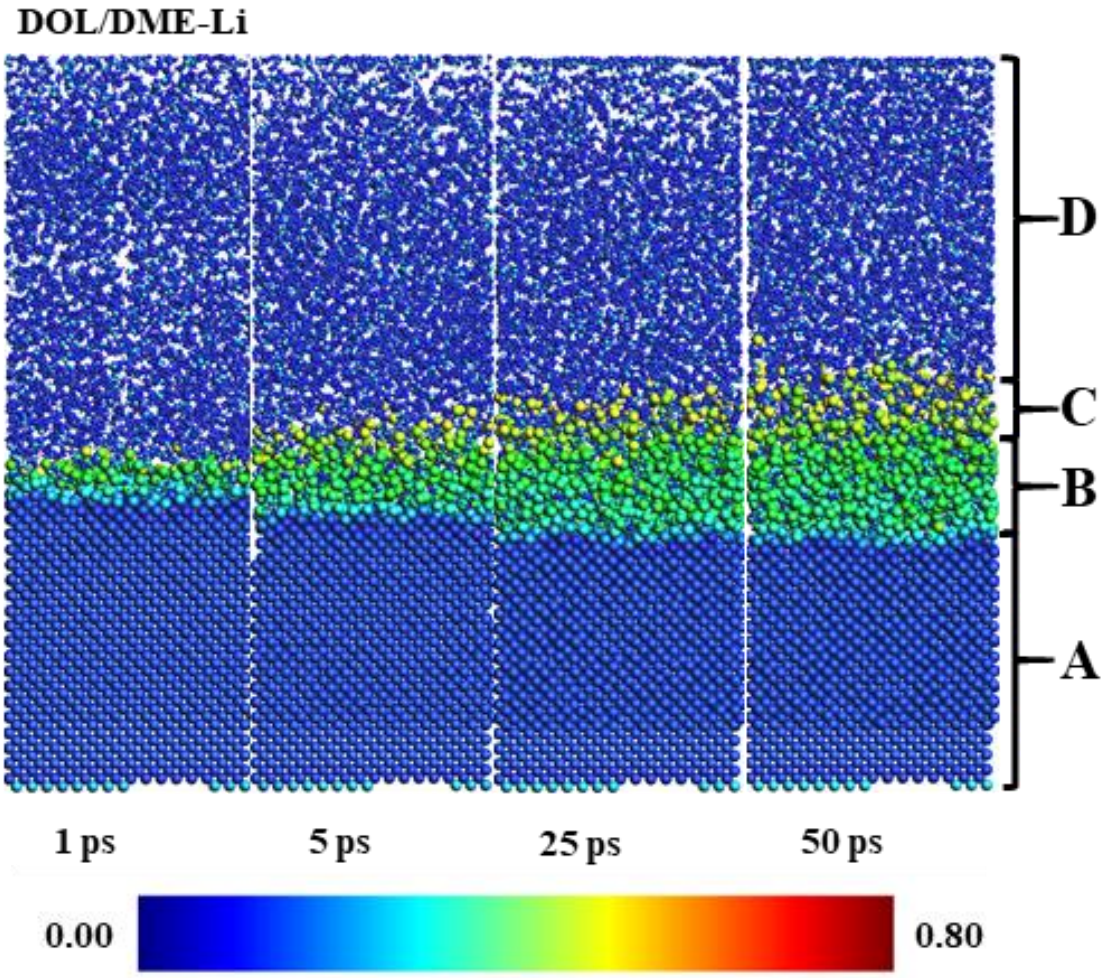

Fig. S4. The simulation snapshot of atomic charges distribution and identification of lithium phases at 1, 5, 25, and 50 ps of simulation time without additives in DOL/DME electrolyte.

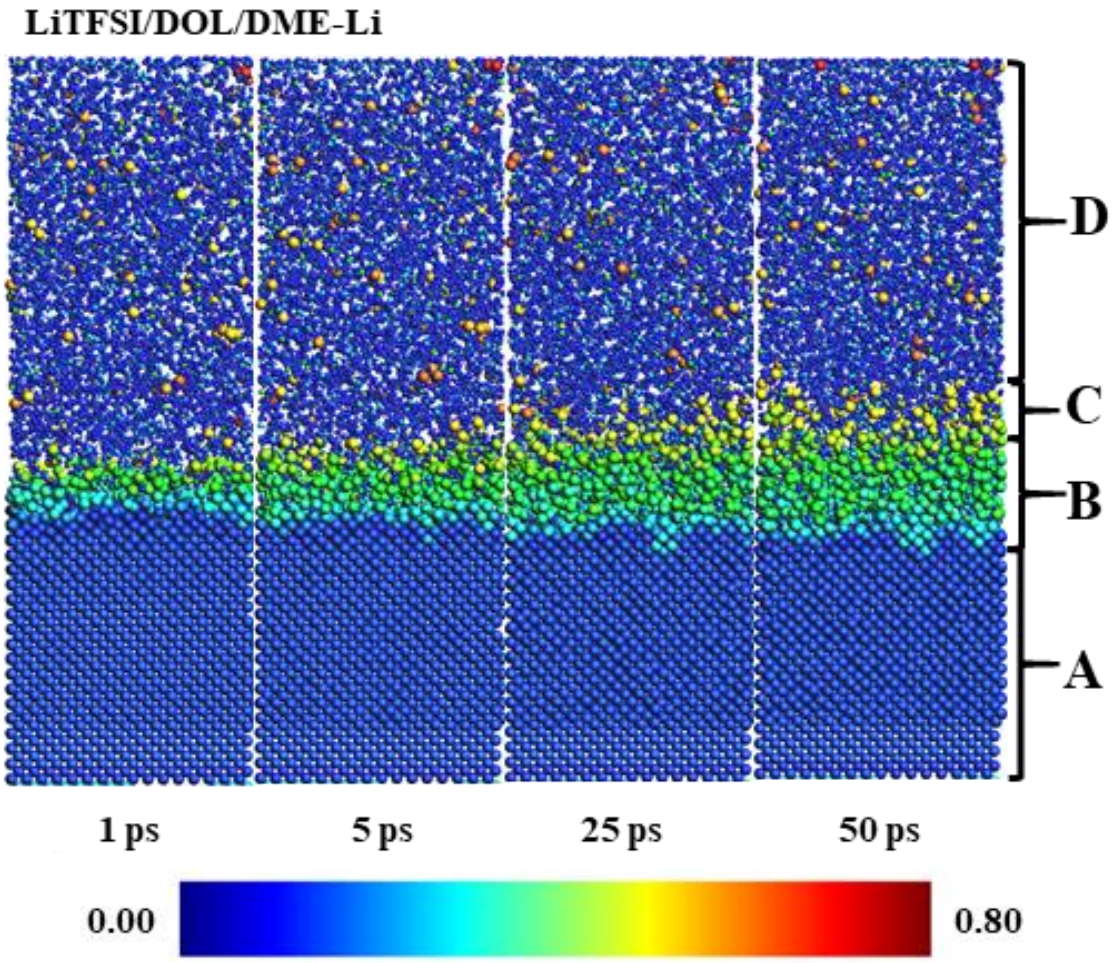

Fig. S5. The simulation snapshot of atomic charges distribution and identification of lithium phases at 1, 5, 25, and 50 ps of simulation time for simulation system LiTFSI/DOL/DME-Li.

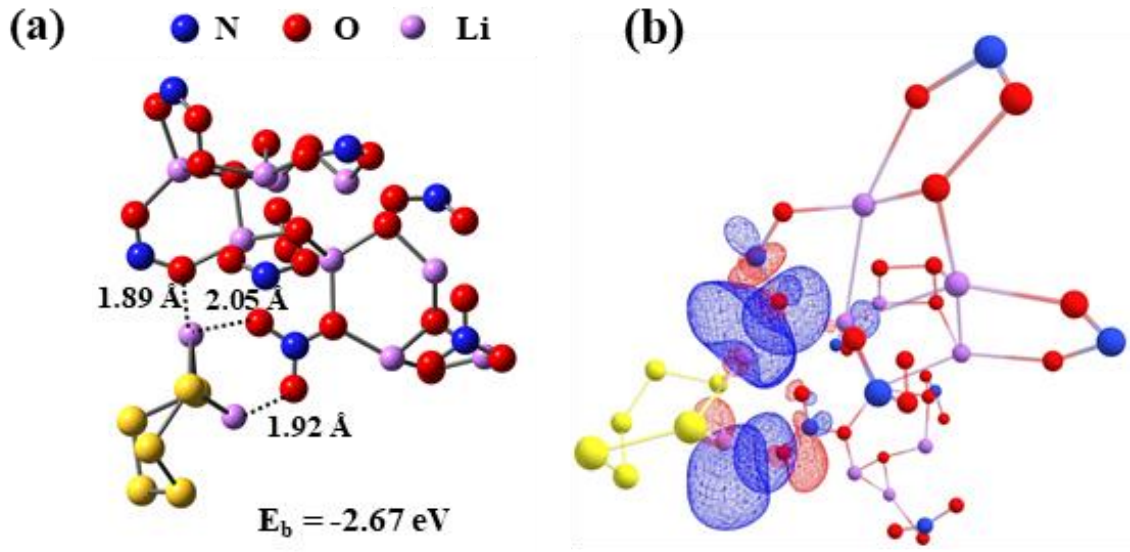

Fig. S6. The natural bond orbital analysis (NBO) based-on M062X/6-31G(d,p) levels of theory of $Li_9N_8O_{26}^{3-}$ with Li_2S_6 molecules.

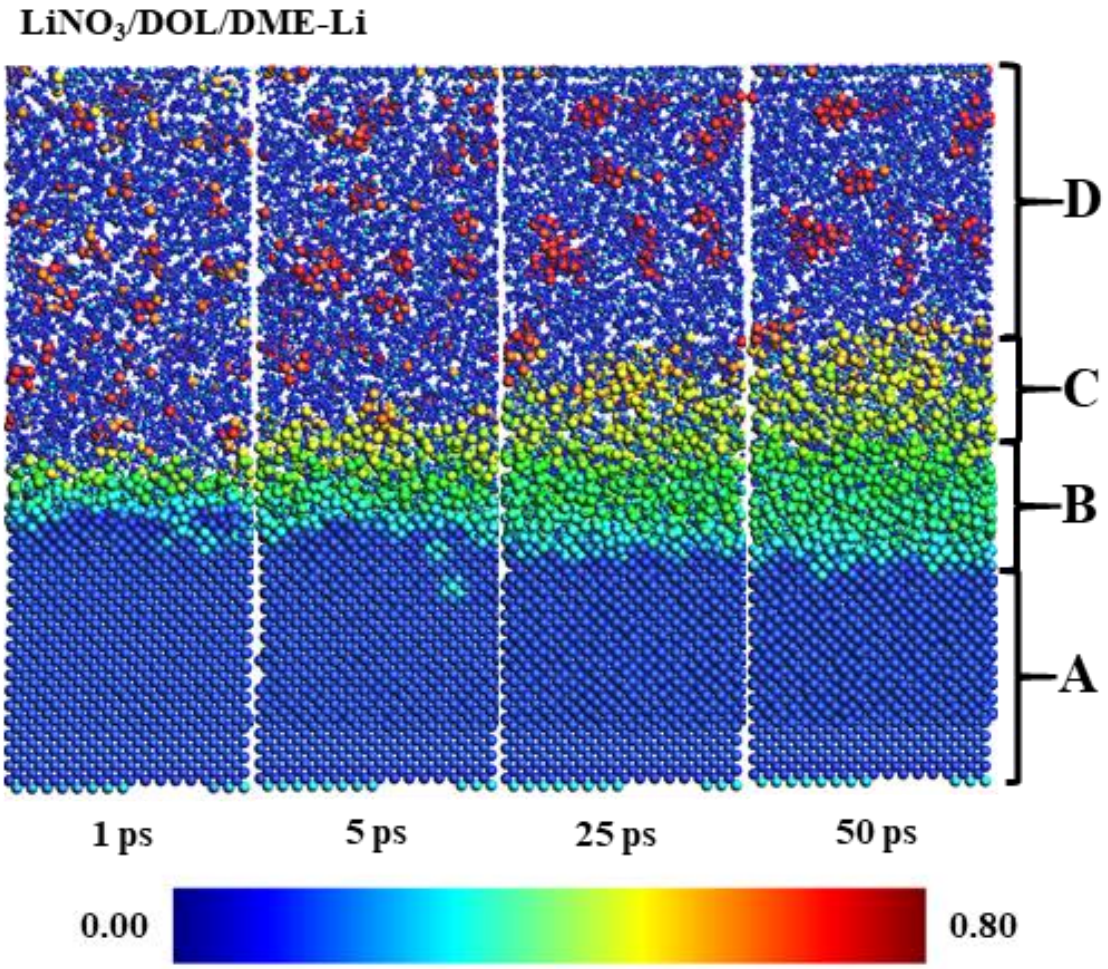

Fig. S7. The simulation snapshot of atomic charges distribution and identification of lithium phases at 1, 5, 25, and 50 ps of simulation time for simulation system $LiNO_3$/DOL/DME-Li.

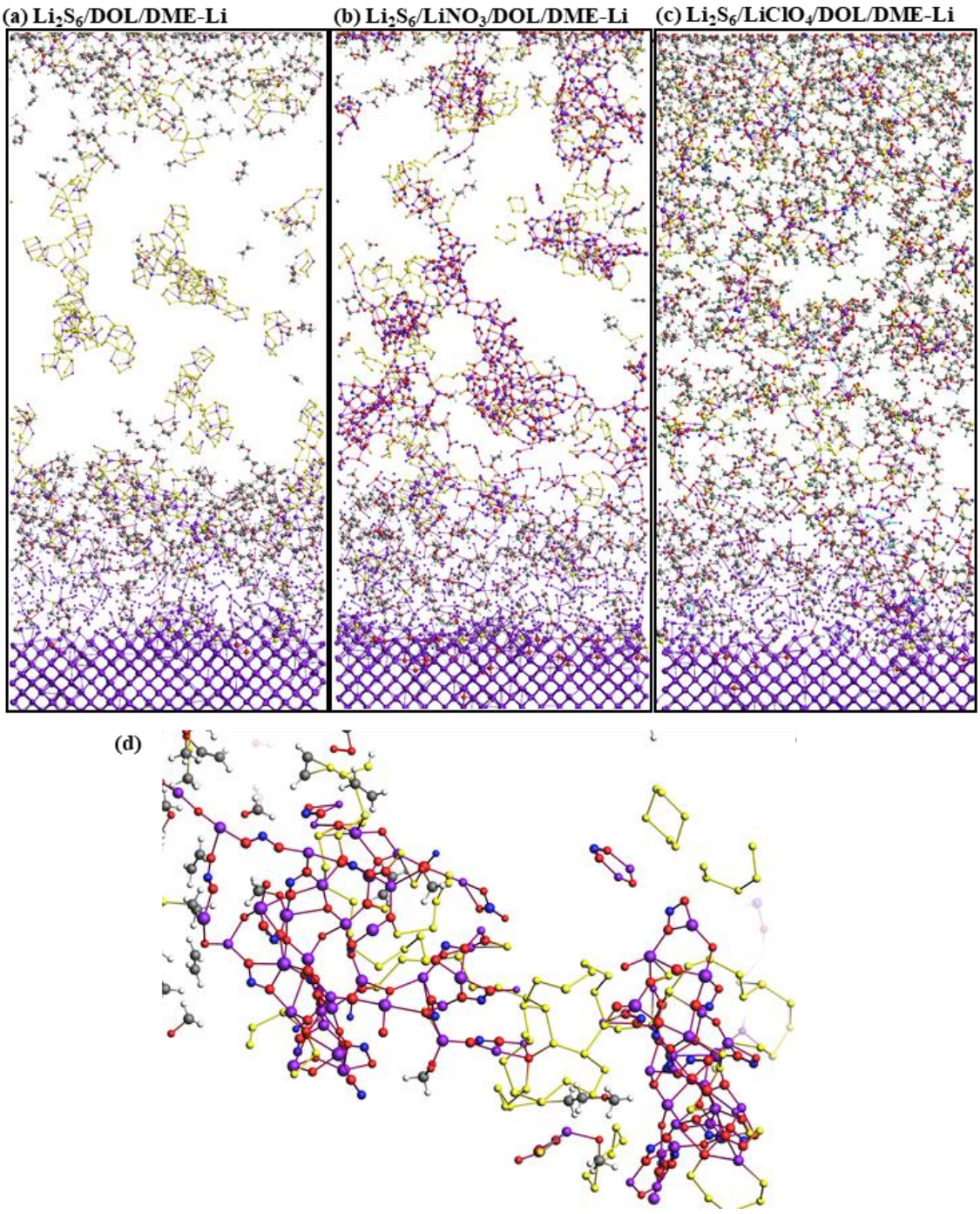

Fig. S8. Components of the cell at 50 ps of simulation time in environment of Li_2S_6 with and without additives (the unreacted DOL/DME molecules were hidden). (a) system Li_2S_6/DOL/DME-Li, (b) system Li_2S_6/$LiNO_3$/DOL/DME-Li, (c) system Li_2S_6/$LiClO_4$/DOL/DME-Li, and (d) high magnification of binding complexes between Li_2S_6 and Li_xNO_y clusters.

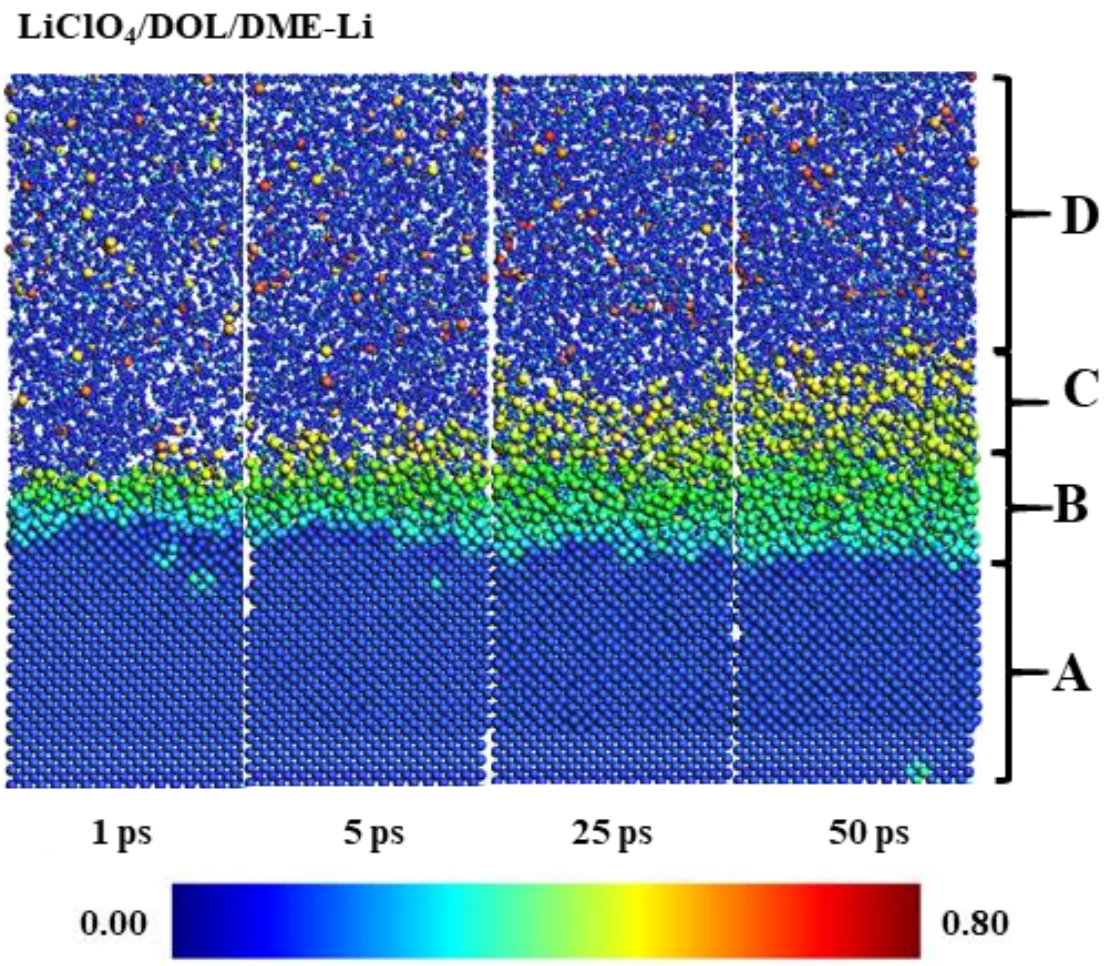

Fig. S9. The simulation snapshot of atomic charges distribution and identification of lithium phases at 1, 5, 25, and 50 ps of simulation time for simulation system $LiClO_4$/DOL/DME-Li.

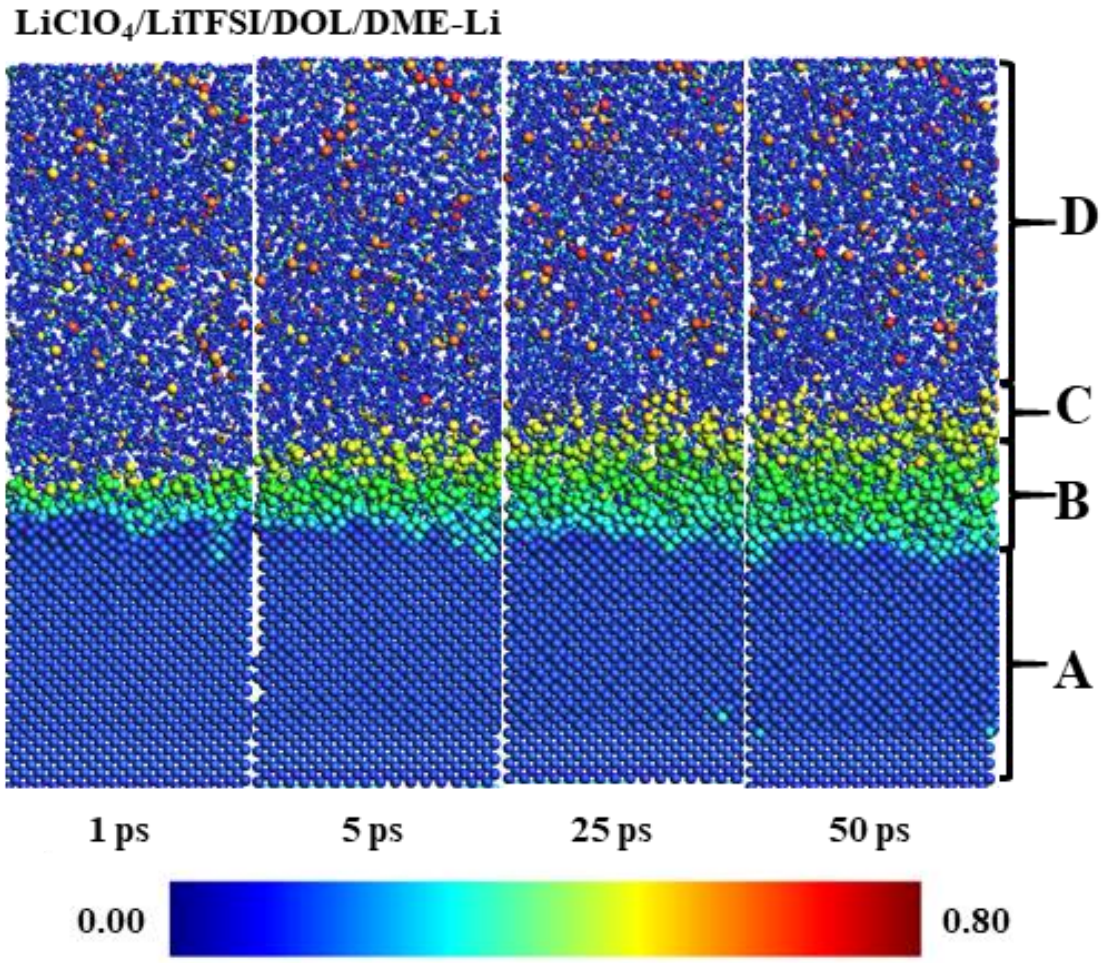

Fig. S10. The simulation snapshot of atomic charges distribution and identification of lithium phases at 1, 5, 25, and 50 ps of simulation time for simulation system $LiClO_4$/LiTFSI/DOL/DME-Li.

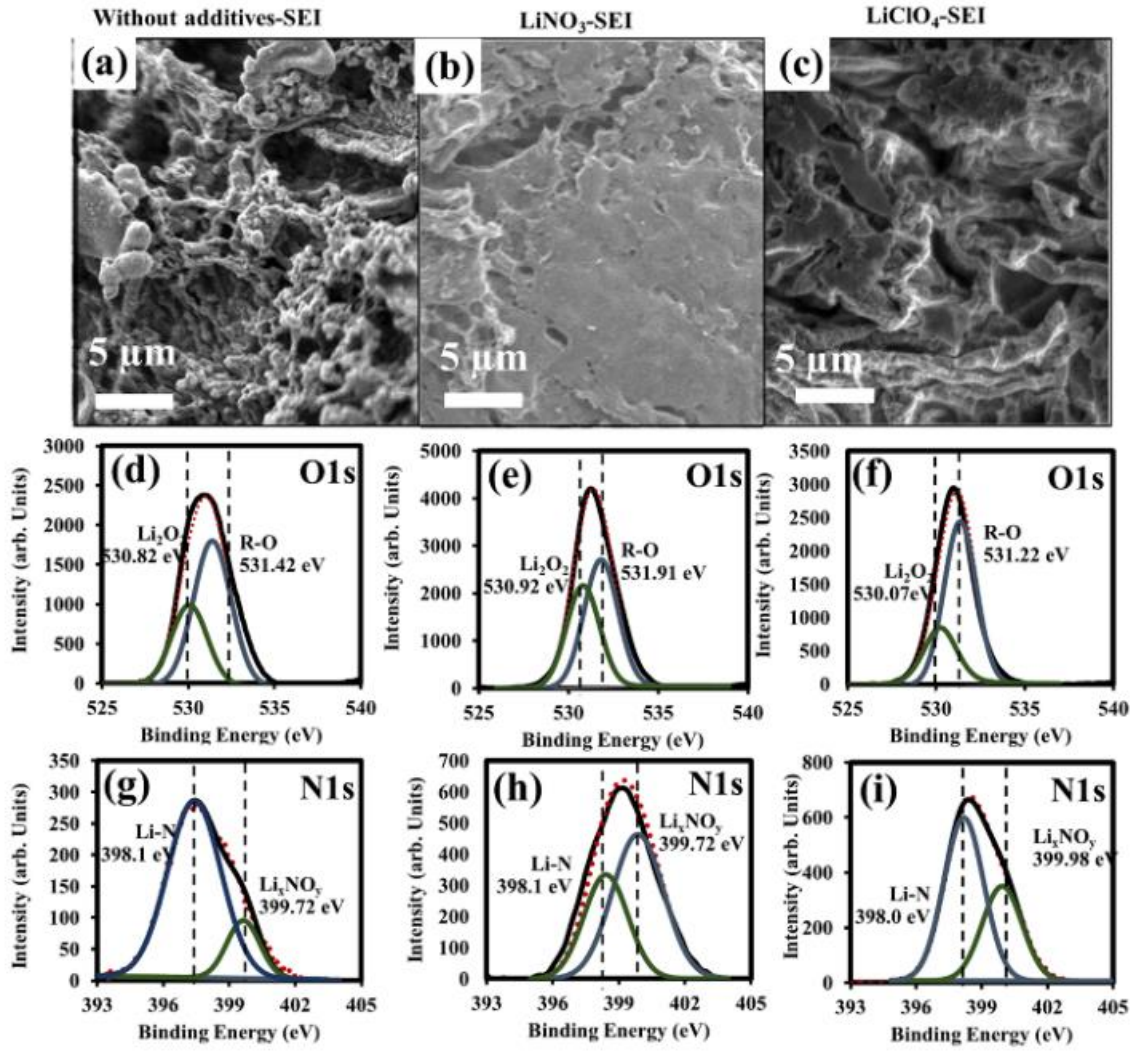

Fig. S11. (a-c) FESEM images of SEI layer after the 50th discharged cycle of LSBs in the absence and presence of additives ($LiNO_3$ and $LiClO_4$), and (d-f) O1s narrow scan and N1s narrow scan XPS spectra of the SEI layers formed at the anode after the 1st discharged in the absence and presence of additives ($LiNO_3$ and $LiClO_4$) of the as-fabricated LSBs.

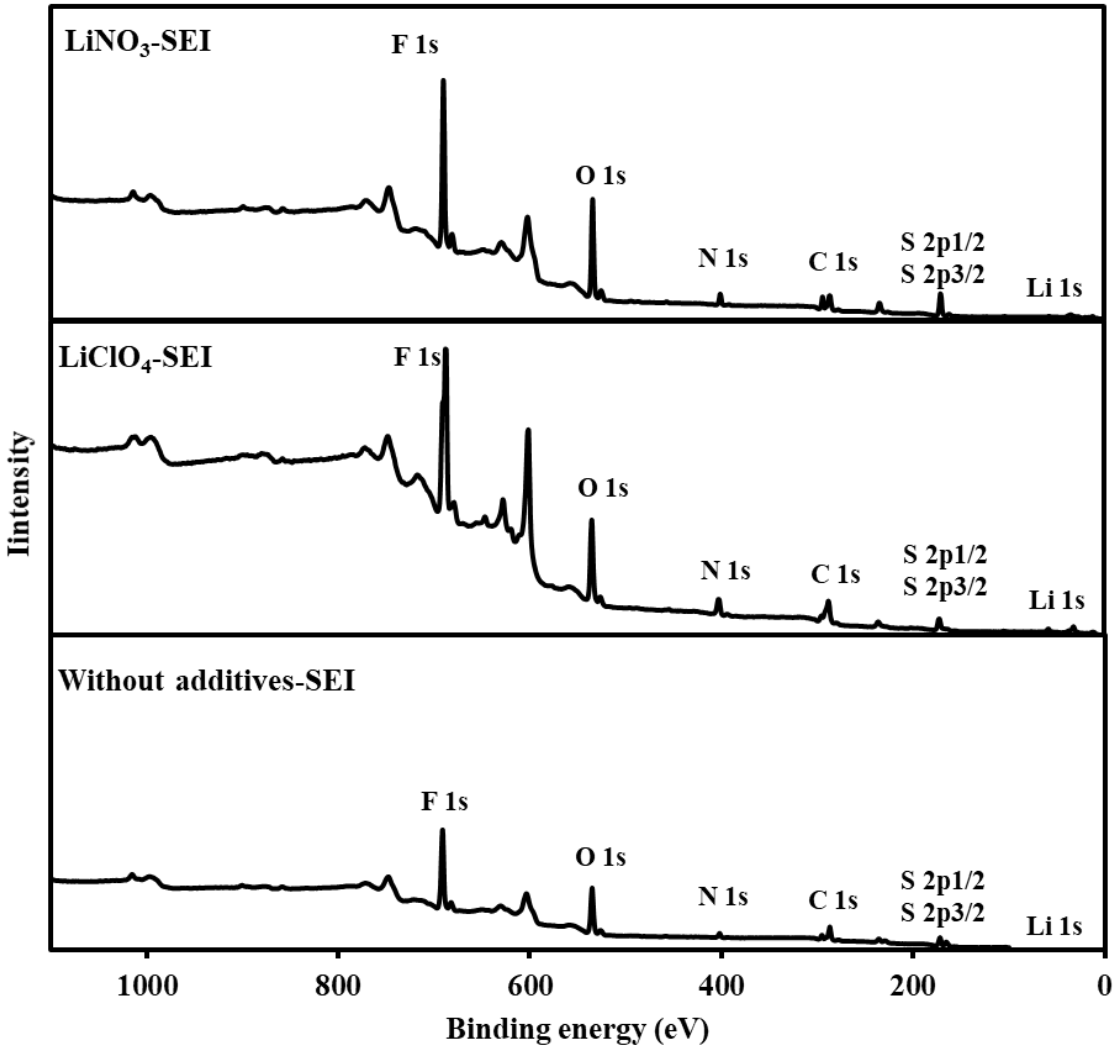

Fig. S12. Wide-scan X-ray photoelectron spectroscopy (XPS) spectra in the range from 0 to 1100 eV.

References

1. A. C. T. van Duin, S. Dasgupta, F. Lorant and W. A. Goddard, *J. Phys. Chem. A*, 2001, **105**, 9396-9409.
2. K. Chenoweth, A. C. T. van Duin and W. A. Goddard, *J. Phys. Chem. A*, 2008, **112**, 1040-1053.
3. M. M. Islam, G. Kolesov, T. Verstraelen, E. Kaxiras and A. C. T. van Duin, *J. Chem. Theory Comput.*, 2016, **12**, 3463-3472.
4. M. M. Islam, V. S. Bryantsev and A. C. T. van Duin, *J. Electrochem. Soc.*, 2014, **161**, E3009-E3014.
5. D. Bedrov, G. D. Smith and A. C. T. van Duin, *J. Phys. Chem. A*, 2012, **116**, 2978-2985.
6. M. M. Islam and A. C. T. van Duin, *J. Phys. Chem. C*, 2016, **120**, 27128-27134.
7. M. R. Nadler and C. P. Kempier, *Anal. Chem.*, 1959, **31**, 2109-2109.
8. S. Nosé, *Mol. Phys.*, 1984, **52**, 255-268.
9. M. J. Frisch, G. W. Trucks, H. B. Schlegel, G. E. Scuseria, M. A. Robb, J. R. Cheeseman, G. Scalmani, V. Barone, G. A. Petersson, H. Nakatsuji, X. Li, M. Caricato, A. V. Marenich, J. Bloino, B. G. Janesko, R. Gomperts, B. Mennucci, H. P. Hratchian, J. V. Ortiz, A. F. Izmaylov, J. L. Sonnenberg, Williams, F. Ding, F. Lipparini, F. Egidi, J. Goings, B. Peng, A. Petrone, T. Henderson, D. Ranasinghe, V. G. Zakrzewski, J. Gao, N. Rega, G. Zheng, W. Liang, M. Hada, M. Ehara, K. Toyota, R. Fukuda, J. Hasegawa, M. Ishida, T. Nakajima, Y. Honda, O. Kitao, H. Nakai, T. Vreven, K. Throssell, J. A. Montgomery Jr., J. E. Peralta, F. Ogliaro, M. J. Bearpark, J. J. Heyd, E. N. Brothers, K. N. Kudin, V. N. Staroverov, T. A. Keith, R. Kobayashi, J. Normand, K. Raghavachari, A. P. Rendell, J. C. Burant, S. S. Iyengar, J. Tomasi, M. Cossi, J. M. Millam, M. Klene, C. Adamo, R. Cammi, J. W. Ochterski, R. L. Martin, K. Morokuma, O. Farkas, J. B. Foresman and D. J. Fox, *Rev. B*, 2016.
10. J. P. Perdew, K. Burke and M. Ernzerhof, *Phys. Rev. Lett.*, 1996, **77**, 3865-3868.
11. Y. Zhao and D. G. Truhlar, *J. Phys. Chem. A*, 2004, **108**, 6908-6918.
12. S. F. Boys and F. Bernardi, *Mol. Phys.*, 1970, **19**, 553-566.
13. A. E. Reed, L. A. Curtiss and F. Weinhold, *Chem. Rev.*, 1988, **88**, 899-926.
14. T. Maihom, S. Kaewruang, N. Phattharasupakun, P. Chiochan, J. Limtrakul and M. Sawangphruk, *J. Phys. Chem. C*, 2018, **122**, 7033-7040.